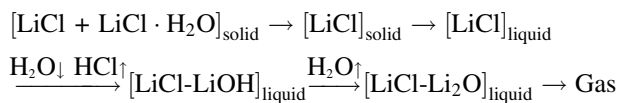


# Thermokinetic characteristics of lithium chloride

Ali Reza Kamali · Derek J. Fray · Carsten Schwandt

Received: 28 June 2010/Accepted: 7 September 2010/Published online: 23 September 2010  
© Akadémiai Kiadó, Budapest, Hungary 2010

**Abstract** The characterisation of the ionic compound of lithium chloride, LiCl, through XRD, SEM, DSC, TG, DTG and TG-MS analysis is reported. The results show that nominally anhydrous LiCl particles can readily absorb water from the ambient atmosphere to form a surface layer of lithium chloride mono-hydrate, LiCl·H<sub>2</sub>O. Solid surface-hydrated LiCl is de-dehydrated via a two-stage mechanism at low heating rates and via a single-stage mechanism at high heating rates. Molten LiCl exhibits substantial evaporation at temperatures below its nominal boiling point, with the rate of evaporation increasing significantly before complete evaporation occurs. The melting process of dehydrated LiCl is marginally affected by the heating rate; whilst the evaporation process is strongly affected by the heating rate and also dependent on the quantity of material used and the flow rate of the gas passed over it. Heating of surface-hydrated LiCl up to the point of evaporation under a flow of argon and under a flow of ambient air gives identical results, proposing the possibility of performing LiCl-based processes in an air environment. The enthalpies and activation energies for the processes of surface dehydration, melting, and high-temperature evaporation are determined. The results are consistent with the following thermal phase evolution:



**Keywords** Lithium chloride · Thermal analysis · De-hydration · Melting · Hydrolysis · Evaporation · Activation energy

## Introduction

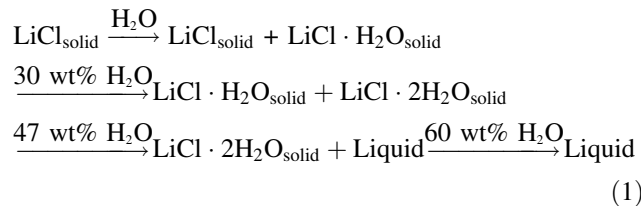
Lithium chloride, LiCl, is an important ionic compound that finds use in a variety of industrial applications. Most prominently, LiCl is the feed material in the electrolytic production of lithium metal [1], serves as the electrolyte in the re-processing of spent nuclear fuel [2–4], and is employed as a flux in aluminium brazing [1]. Like most lithium-based salts, LiCl is characterised by a relatively low melting point and high ionic conductivity which render it a suitable component in molten salt electrolytes for thermal batteries [5, 6].

It is generally known that, at room temperature, lithium ions with a diameter of 0.073 nm may be reversibly electro-intercalated into and de-intercalated from the interlayer spacings of graphite with a layer distance of 0.335 nm. This qualifies this system for use as the negative electrode in lithium ion batteries and capacitors [7, 8]. More recent investigations have shown that intercalation of lithium into graphite may also proceed at elevated temperatures as high as 625 to 900 °C [9–12]. This forms the basis of an emerging process for the preparation of nano-structured carbon materials, including multi-walled carbon nanotubes, in which molten LiCl is electrolysed with graphite electrodes [13–15].

There are, however, some limitations regarding the straightforward usage of LiCl in its applications in that LiCl is very sensitive to moisture and will easily absorb water in humid atmosphere. Because of this LiCl has been considered as a humidistat for the drying of gases [16]. According to the phase diagram of the LiCl-H<sub>2</sub>O system, presented in Fig. 1

A. R. Kamali (✉) · D. J. Fray · C. Schwandt  
Department of Materials Science and Metallurgy, University of Cambridge, Pembroke Street, Cambridge CB2 3QZ, UK  
e-mail: ark42@cam.ac.uk; alirezakam@yahoo.com

[17], LiCl forms a number of well-defined hydrates in the presence of water at different temperatures. For example, hydration of LiCl at temperatures between about  $-20$  and  $20$  °C can be depicted as shown in Eq. 1.



Consequently, handling of LiCl in air is generally avoided, and processes using this material are typically carried out under a protective atmosphere of gases such as argon, which adds significantly to the cost at industrial scale.

It is evident that comprehensive knowledge about the thermal behaviour of LiCl is required in order to be able to evaluate the technical and economic aspects of its usage. However, despite its importance, only very little scientific information has been published on the thermal behaviour of LiCl, especially when used in the absence of a protective atmosphere. Recently, Masset studied the thermal behaviour of lithium chloride mono-hydrate,  $\text{LiCl}\cdot\text{H}_2\text{O}$ , under dry helium gas by thermal analysis up to a temperature of about  $620$  °C [18]. It was found that  $\text{LiCl}\cdot\text{H}_2\text{O}$  dehydrates in a two-step reaction between  $99$  and  $186$  °C, and it was also shown that the melting point of the dehydrated material is identical with that of pure LiCl, suggesting that thermal dehydration does not lead to residual impurities. However, there is still a need to investigate the thermal behaviour of LiCl in more detail at higher temperatures and under different atmospheres. One aim of the present study

has been to evaluate the thermal behaviour of LiCl up to the temperature of  $1,300$  °C, both under a flow of argon and under a flow of ambient air; and a further goal has been to determine several thermodynamic and kinetic parameters, including the enthalpies and the activation energies of de-hydration, melting and evaporation.

## Experimental

Nominally anhydrous LiCl (213233, Sigma–Aldrich) of purity greater than 99% was selected for the present study. In all investigations, the as-received material was taken from the original container, kept in a sealed bag, and analysed without unnecessary delay. A Philips 1710 high-resolution X-ray diffractometer (XRD) with Cu anode was employed for phase identification. A JEOL 6340F field emission scanning electron microscope (SEM) was used for microstructural investigations. An SDT Q600 analyser equipped with alumina crucibles was used for various thermoanalytical analyses, including differential scanning calorimetry (DSC), thermal gravimetry (TG), and differential thermal gravimetry (DTG). A Pfeiffer Vacuum ThermoStar™ gas analysis system coupled with a TA Instruments Q500 Thermogravimetric Analyzer was used for simultaneous thermogravimetry-mass spectrometry (TG-MS) of evolved gas. The enthalpies of the various phenomena giving rise to peaks on the thermoanalytical curves were determined from integration of the respective sections of the DCS traces, and the activation energies were calculated from the dependence of peak temperature on heating rate using the well-known Kissinger approach [19, 20], as expressed in Eq. 2.

$$\ln\left(\frac{B}{T_p^2}\right) = -\frac{E_c}{RT_p} + \text{constant} \quad (2)$$

where  $B$  is the heating rate,  $T_p$  is the temperature at the specific peak,  $E_c$  is the activation energy and  $R$  is the universal gas constant. The Kissinger method is generally accepted for the analysis of thermally activated processes from thermoanalytical measurements, and satisfying results have been reported [21, 22]. The enthalpies and Gibbs free energies of selected reactions were calculated using HSC Chemistry 5.0 [23].

## Results and discussion

### Structural and morphological characterisation of lithium chloride

The as-received LiCl material was subjected to XRD analysis in order to determine phase composition. A spectrum

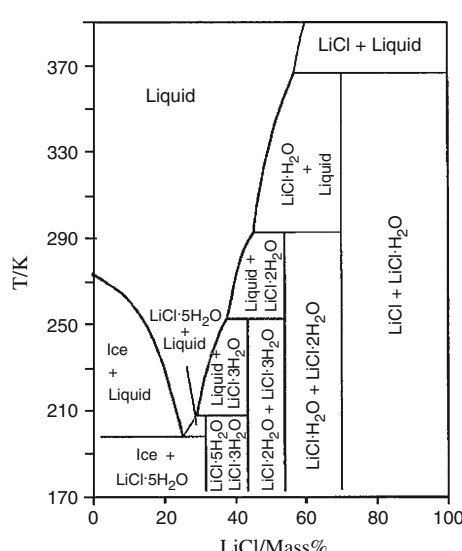


**Fig. 1** Phase diagram of LiCl-H<sub>2</sub>O, adapted with permission from [17], Copyright 2002 American Chemical Society

recorded in ambient air is presented in Fig. 2. Phase analysis indicates that anhydrous LiCl is the majority component in the material, while a minor amount of monohydrate  $\text{LiCl}\cdot\text{H}_2\text{O}$  is clearly visible. The result shows that LiCl has a strong tendency to absorb and retain water.

More information about the LiCl material used was obtained from SEM examination. A typical micrograph is shown in Fig. 3. The image reveals that dark particles with a diameter of several micrometres are interconnected by thin bright layers with a thickness in the sub-micrometre range. It is straightforward to assume that the layers are composed of  $\text{LiCl}\cdot\text{H}_2\text{O}$  that is formed through absorption of water at the surface of the anhydrous LiCl particles. This interpretation makes the results from XRD and SEM analyses fully consistent.

The above experimental observations are also in accordance with predictions based on the phase diagram in Fig. 1 which shows that  $\text{LiCl}\cdot\text{H}_2\text{O}$  is the first hydrate to form when anhydrous LiCl is exposed to humidity. A further observation was that the LiCl material, when exposed to air for long periods of time at ambient conditions, became increasingly sticky and noticeably wet on the surface. In view of the phase transitions this indicates the consecutive formation of higher hydrates and the eventual dissolution of the LiCl in its own crystal water.

#### Thermoanalytical characterisation of lithium chloride under argon

DSC and TG analyses were performed with approximately 20 mg of LiCl heated at a rate of  $40\text{ }^\circ\text{C min}^{-1}$  under high-purity argon of flow rate  $100\text{ mL min}^{-1}$ . Figure 4 displays the results. On the DSC curve four endothermic peaks are discernible. The first peak occurs at a temperature of  $110\text{ }^\circ\text{C}$  and may be attributed to surface de-hydration of the LiCl. This step is accompanied by a 2.57% reduction in total mass. The second peak occurs at a temperature of  $617\text{ }^\circ\text{C}$  and can be assigned to the melting of pure LiCl. The total mass loss up to around  $600\text{ }^\circ\text{C}$  is 2.72%. As

evaporation of LiCl only becomes significant at temperatures in excess of the melting point, the results suggest that the entire mass loss before melting is due to water evaporation, with 94% of the initial total water content exiting the material at around  $110\text{ }^\circ\text{C}$  and the remainder being released gradually at higher temperatures. Subsequent to the melting process, there is a small peak at  $835\text{ }^\circ\text{C}$ , followed by a large peak that terminates sharply at  $1,169\text{ }^\circ\text{C}$ . These peaks are accompanied by the onset of an extensive mass loss, and it is straightforward to attribute this to the evaporation of the LiCl.

In order to study the evaporation process of LiCl in more detail, a DTG curve is presented in Fig. 5a and the high-temperature section of a TG curve in Fig. 5b. It is clear from Fig. 5a that an extensive mass loss sets at  $820\text{ }^\circ\text{C}$  and continues up to  $1,169\text{ }^\circ\text{C}$  where the entire material has evaporated. As may be determined by linear regression of the data in Fig. 5b, the rate of evaporation is approximately independent of temperature in the range from  $820$  to  $900\text{ }^\circ\text{C}$ , with a constant value of  $0.016\text{ mg }^\circ\text{C}^{-1}$  ( $0.08\% \text{ }^\circ\text{C}^{-1}$ ), and then increases progressively beyond  $900\text{ }^\circ\text{C}$ , reaching an ultimate value of as high as  $0.11\text{ mg }^\circ\text{C}^{-1}$  ( $0.54\% \text{ }^\circ\text{C}^{-1}$ ) as the temperature of  $1,169\text{ }^\circ\text{C}$  is approached.

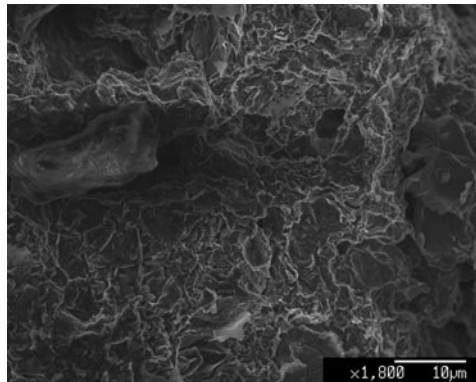


**Fig. 3** SEM image of LiCl as employed in this study

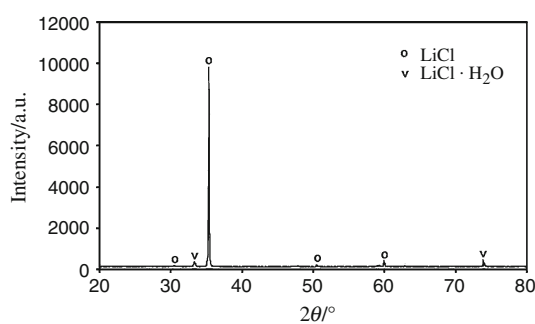


**Fig. 2** X-ray diffraction pattern of LiCl as employed in this study

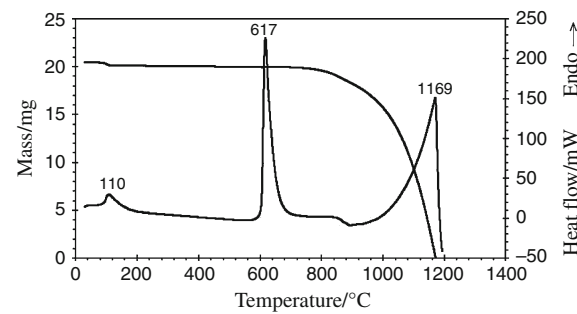


**Fig. 4** DSC and TG curves for 20 mg of LiCl heated at a rate of  $40\text{ }^\circ\text{C min}^{-1}$  under an argon flow of  $100\text{ mL min}^{-1}$

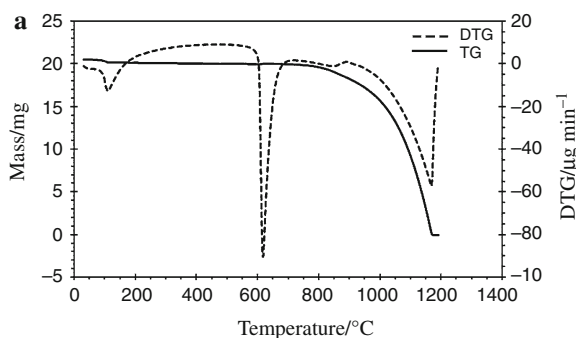


**Fig. 5** **a** TG/DTG curves and **b** section of TG curve at higher resolution for 20 mg of LiCl heated at a rate of  $40\text{ }^{\circ}\text{C min}^{-1}$  under an argon flow of  $100\text{ mL min}^{-1}$

#### Thermoanalytical characterisation of lithium chloride under ambient air

DSC and TG curves were recorded with approximately 20 mg of LiCl heated at a rate of  $40\text{ }^{\circ}\text{C min}^{-1}$  under ambient air of flow rate  $100\text{ mL min}^{-1}$ . The DSC curve is shown in Fig. 6, together with a DSC curve obtained under a flow of argon at otherwise identical conditions. It is obvious that the DSC curves for heating LiCl under ambient air and argon are virtually identical. This result is of potential practical interest, as it indicates the possibility of replacing an inert gas atmosphere with an air atmosphere in processes employing molten LiCl at elevated temperatures, which would offer economic benefits without compromising the characteristics of the molten salt.

For a more detailed analysis, TG and DTG curves of LiCl heated under ambient air are plotted in Fig. 7a and b. It is found that a 3.06% mass loss occurs at the temperature of  $108\text{ }^{\circ}\text{C}$  while the total mass loss up to  $600\text{ }^{\circ}\text{C}$  amounts to 3.59%. Hence, 85% of the total water content is removed from the material at  $108\text{ }^{\circ}\text{C}$  and the rest is released gradually at higher temperatures. The different percentages of water loss of 95 and 85% at surface de-hydration temperature, as measured for heating under argon and ambient air, respectively, may be attributed to the finite water partial pressure in air which is likely to retard water release. Nevertheless, comparison of Figs. 5 and 7 reveals that the

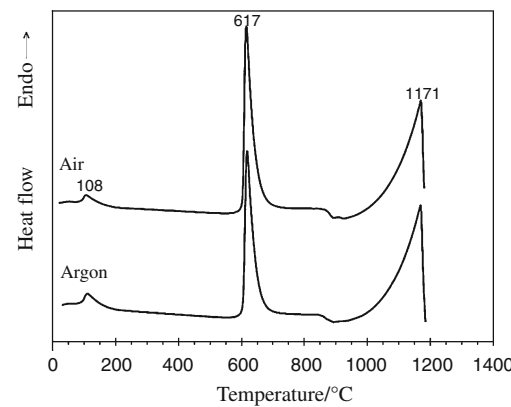


**Fig. 6** DSC curves for 20 mg of LiCl heated at a rate of  $40\text{ }^{\circ}\text{C min}^{-1}$  under an ambient air flow of  $100\text{ mL min}^{-1}$  and an argon flow of  $100\text{ mL min}^{-1}$

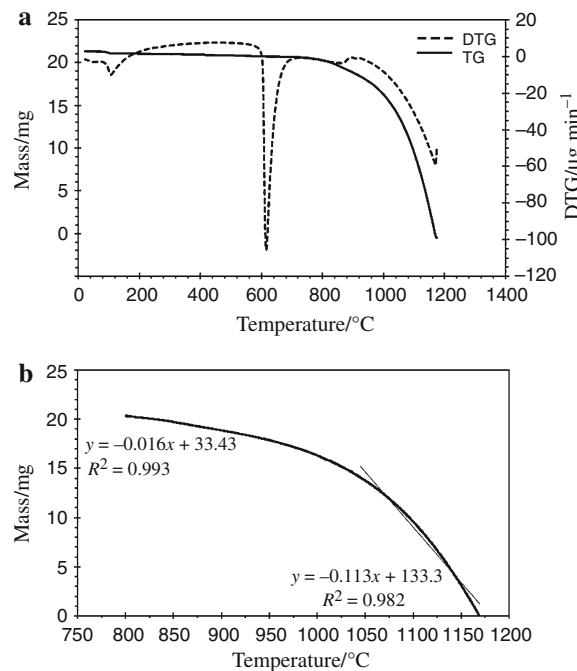


**Fig. 7** **a** TG/DTG curves and **b** section of TG curve at higher resolution for 20 mg of LiCl heated at a rate of  $40\text{ }^{\circ}\text{C min}^{-1}$  under an ambient air flow of  $100\text{ mL min}^{-1}$

same regimes of water loss from LiCl exist during both heating under argon and air.

#### Effect of quantity on transition temperatures

DSC analyses were carried out with different amounts of LiCl, ranging from 9 to 42 mg, heated at a rate of  $40\text{ }^{\circ}\text{C min}^{-1}$  under an ambient air flow of  $100\text{ mL min}^{-1}$ . Figure 8 presents the curves recorded. The results indicate that the quantity of material used has no noticeable effect on the melting temperature, i.e., the transition between two

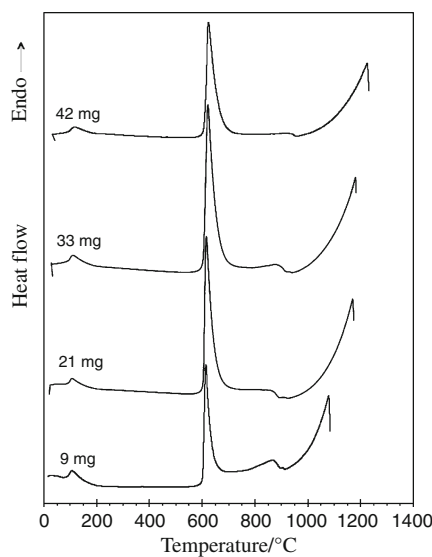


**Fig. 8** DSC curves for different amounts of LiCl, ranging from 9 to 42 mg, heated at a rate of  $40\text{ }^{\circ}\text{C min}^{-1}$  under an ambient air flow of  $100\text{ mL min}^{-1}$

condensed phases. However, the quantity used has an influence on the evaporation behaviour. This can be explained by the fact that evaporation is a surface phenomenon, with molecules located near the liquid/gas interface escaping into the vapour phase, so evaporation will be controlled strongly by the surface-to-volume ratio of the liquid. For higher ratios there is a shorter average distance for the molecules to reach the interface which leads to a higher evaporation rate. It can furthermore be seen that the two-stage mechanism of evaporation tends to change to a one-stage mechanism with increasing quantities.

#### Effect of gas flow rate on transition temperatures

DSC curves were obtained during the heating of 20 mg of LiCl at a rate of  $40\text{ }^{\circ}\text{C min}^{-1}$  under both ambient air of flow rate  $100\text{ mL min}^{-1}$  and static ambient air. The results are shown in Fig. 9. It can be seen that the gas flow rate has no significant effect on the melting temperature but has a considerable impact on the evaporation behaviour. As expected, the evaporation rate is higher under flowing air, which is due to a combination of a thinner diffusion layer and a larger surface area, both resulting from the air impinging the liquid/gas interface.

#### Effect of heating rate on transition temperatures

20 mg of LiCl were analysed by means of DSC at different heating rates, ranging from  $10$  to  $50\text{ }^{\circ}\text{C min}^{-1}$ , and under an ambient air flow of  $100\text{ mL min}^{-1}$ . The results are compiled in Fig. 10. The curve recorded at a heating rate of  $10\text{ }^{\circ}\text{C min}^{-1}$

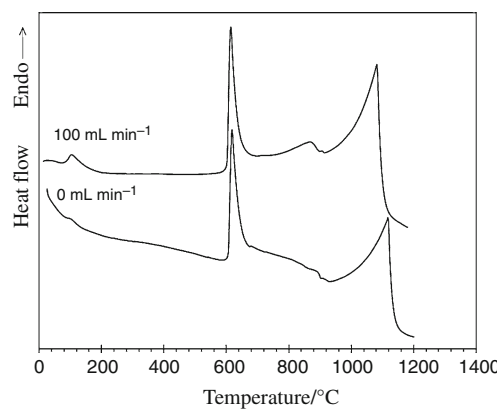
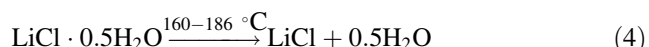


**Fig. 9** DSC curves for 20 mg of LiCl heated at a rate of  $40\text{ }^{\circ}\text{C min}^{-1}$  under ambient air of flow rate  $100\text{ mL min}^{-1}$  and static ambient air

$\text{min}^{-1}$  exhibits two endothermic peaks for surface de-hydration of LiCl at the temperatures of  $47$  and  $93\text{ }^{\circ}\text{C}$ . The occurrence of two peaks is in qualitative agreement with the two-stage mechanism for bulk de-hydration of  $\text{LiCl}\cdot\text{H}_2\text{O}$  proposed by Masset [18], who found two endothermic peaks at  $99\text{--}110$  and  $160\text{--}186\text{ }^{\circ}\text{C}$  in DTA curves of  $\text{LiCl}\cdot\text{H}_2\text{O}$  at heating rates of, or less than,  $10\text{ }^{\circ}\text{C min}^{-1}$ . These were attributed to the following reactions:



It is moreover seen from Fig. 10 that when increasing the heating rate to values beyond  $10\text{ }^{\circ}\text{C min}^{-1}$ , the first endothermic peak disappears, indicating that surface de-hydration of LiCl proceeds in only one step at higher heating rates. The initial water content of the material was determined by averaging the mass loss in samples heated up to  $600\text{ }^{\circ}\text{C}$  with different heating rates, and was found to be  $2.55\%$  with  $88\%$  thereof being removed below  $120\text{ }^{\circ}\text{C}$ .

The enthalpy of a process giving rise to a peak on a DSC curve may be determined by integrating the area under the peak. Averaging the numbers obtained for different heating rates, the enthalpy of surface de-hydration of LiCl is calculated to be  $1.3\text{ kJ mol}^{-1}$ . Similarly, the enthalpy of melting of LiCl is found to be  $22.1\text{ kJ mol}^{-1}$ , which is in good agreement with the value of  $19.7\text{ kJ mol}^{-1}$  reported in the literature [24], and the enthalpy of high-temperature evaporation is found to be  $131.4\text{ kJ mol}^{-1}$ .

The activation energy of the respective processes can be determined according to Eq. 2. Specific peak temperatures for surface de-hydration, melting and complete evaporation of LiCl at different heating rates are compiled in Table 1. It can be seen that the peak temperatures of all transitions increase with rising heating rate, which is a well-established concept [19–22].

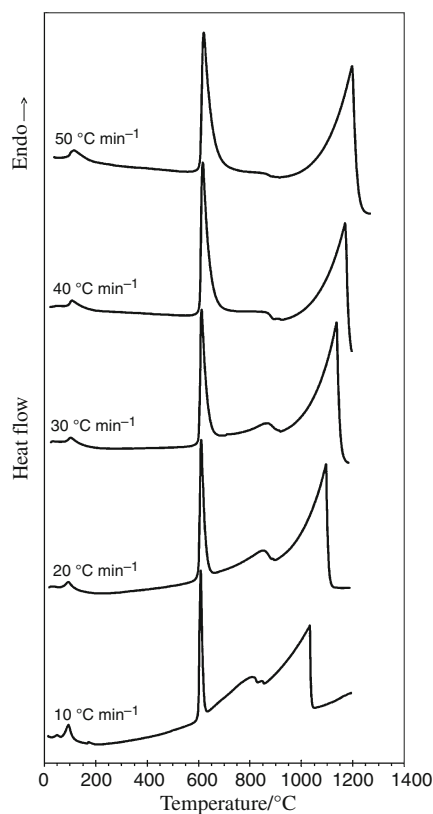


**Fig. 10** DSC curves for 20 mg of LiCl heated at different rates, ranging from 10 to 50 °C min<sup>-1</sup>, under an ambient air flow of 100 mL min<sup>-1</sup>

**Table 1** Transition temperatures for surface de-hydration, melting and complete evaporation of LiCl at different heating rates under an ambient air flow of 100 mL min<sup>-1</sup> (For surface de-hydration at 10 °C min<sup>-1</sup> only the de-hydration step at the higher temperature is considered)

	Heating rate/°C min <sup>-1</sup>				
	10	20	30	40	50
Temperature of surface de-hydration/°C	93.3	93.7	104.1	107.8	114.8
Temperature of melting/°C	608.1	610.4	612.0	616.7	620.7
Temperature of complete evaporation/°C	1032.5	1093.1	1133.5	1171.0	1195.4

Figure 11 shows a graphic representation of the data in Table 1. From the figure the activation energy of surface de-hydration of LiCl is determined to be 68.2 kJ mol<sup>-1</sup>. Masset [18] found that the second step of bulk de-hydration of LiCl·H<sub>2</sub>O occurs at a temperature of 186 °C at the same heating rate and calculated an activation energy of 137 kJ mol<sup>-1</sup>. The difference between the numbers obtained in both studies can be explained through the different mechanisms that govern the respective de-hydration processes. In the case of de-hydration of bulk LiCl·H<sub>2</sub>O,

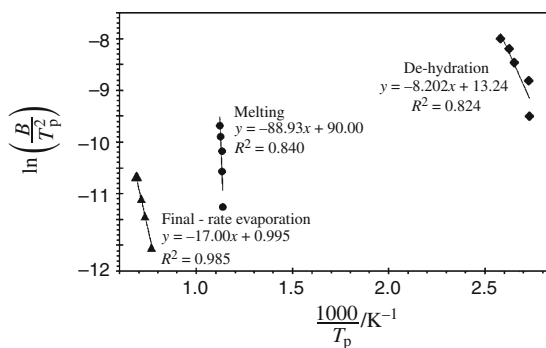


**Fig. 11** Plots of  $\ln\left(\frac{B}{T_p^2}\right)$  vs.  $\frac{1000}{T_p}$  for surface de-hydration, melting and complete evaporation of LiCl

**Table 2** Enthalpies and activation energies for surface de-hydration, melting and high-temperature evaporation of LiCl

	Surface de-hydration	Melting	High-temperature evaporation
Enthalpy/kJ mol <sup>-1</sup>	1.3	22.1	131.4
Activation energy/kJ mol <sup>-1</sup>	68.2	739.4	64.8

H<sub>2</sub>O molecules need to transport through the volume of a particle before evaporating from the surface. In contrast, de-hydration of a surface layer of LiCl·H<sub>2</sub>O around anhydrous LiCl particles does not require significant prior transport of H<sub>2</sub>O, and may thus proceed at lower temperature and with lower activation energy. The figure also shows that the activation energy of melting of LiCl is 739.4 kJ mol<sup>-1</sup> and that the activation energy of high-temperature evaporation is 64.8 kJ mol<sup>-1</sup>. The square of the linear correlation coefficient,  $R^2$ , is an indication of how closely the regression lines fit the measured data. The values obtained for de-hydration, melting and final-rate evaporation suggest that the Kissinger equation, which is based on the assumption of constant activation energy, is conceptually able to describe these transitions during the heating of LiCl.

The data of the enthalpies and the activation energies for the various transition processes discussed above are summarised in Table 2.

### Evaporation mechanism

According to Figs. 4, 6, 8, 9 and 10, melting of LiCl takes place at temperatures that are in good agreement with the literature value of about 610 °C [18]. In contrast, the generally quoted boiling point of LiCl of 1,360 °C is significantly higher than the temperatures of around 1,200 °C

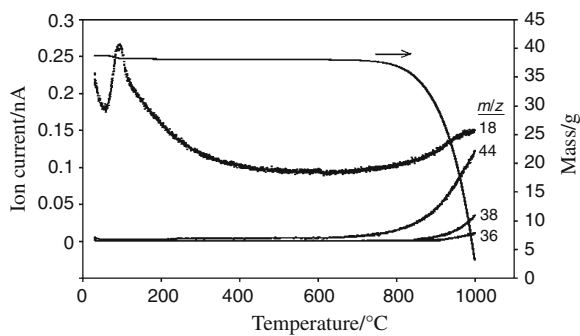


**Fig. 12** TG-MS analysis of 20 mg of LiCl heated at a rate of  $10\text{ }^{\circ}\text{C min}^{-1}$  under an ambient air flow of  $60\text{ mL min}^{-1}$

that have been found sufficient to allow for complete evaporation in the present study. In what follows it will be attempted to elucidate the reasons for this behaviour.

Figure 12 shows a TG-MS analysis of 20 mg of LiCl during heating at a rate of  $10\text{ }^{\circ}\text{C min}^{-1}$  under an ambient air flow of  $60\text{ mL min}^{-1}$ . The mass-to-charge ratio,  $m/z$ , of 18 is attributed to the  $\text{H}_2\text{O}^+$  ion, and the  $m/z$  ratio of 44 is attributed to the  $\text{LiCl}^+$  ion containing the  $^{37}\text{Cl}$  isotope. The  $m/z$  ratios of 38 and 36 are indicative of the  $\text{HCl}^+$  ion including the  $^{37}\text{Cl}$  and  $^{35}\text{Cl}$  isotopes, respectively. The figure confirms water release during surface de-hydration of LiCl at low temperature, and there is furthermore an indication of water release at high temperatures of above  $800\text{ }^{\circ}\text{C}$ . Evaporation of LiCl is seen to commence at a minor rate at temperatures beyond about  $650\text{ }^{\circ}\text{C}$ , and then slowly accelerates up to  $800\text{ }^{\circ}\text{C}$  where a sharp rise occurs. Release of HCl can be detected at temperatures in excess of  $800\text{ }^{\circ}\text{C}$ .

The information obtained from Fig. 12 may be used to explain the small endothermic peaks observed in the DSC curve in Fig. 10 for the heating rate of  $10\text{ }^{\circ}\text{C min}^{-1}$ . The first endothermic peak at about  $801\text{ }^{\circ}\text{C}$  is caused by the hydrolysis of molten LiCl to LiOH, as expressed by Eq. 5. The reaction involves the experimentally observed release of HCl, with a theoretical mass loss of 39.5% of the mono-hydrated LiCl.



Figure 13 shows the enthalpy and Gibbs free energy for Reaction 5 as a function of temperature. The enthalpy values reveal the endothermic nature of this reaction which is in agreement with the endothermic peak on the DSC curves. The Gibbs free energy of the reaction is positive, yet the reaction may occur at a finite rate in the presence of a flowing gas that continuously removes the gaseous product.

The second endothermic peak at  $831\text{ }^{\circ}\text{C}$  can be attributed to the decomposition of LiOH to  $\text{Li}_2\text{O}$ , as shown in Eq. 6. The reaction involves the release of  $\text{H}_2\text{O}$ , with a theoretical mass loss of 37.6% of the LiOH.

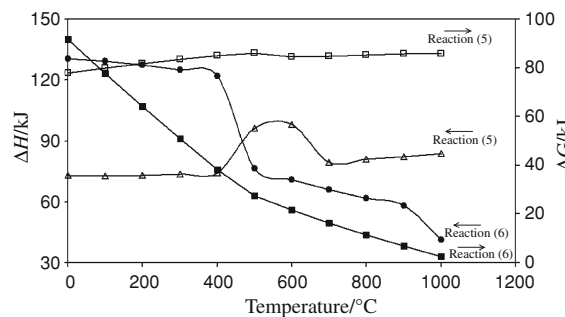


**Fig. 13** Changes of molar enthalpy and molar Gibbs free energy of Reactions 5 and 6



The enthalpy values for Reaction 6, also shown on Fig. 13, indicate that this reaction is endothermic, which is in line with the endothermic peak observed on the DSC curves. The Gibbs free energy of the reaction is again positive, but can proceed in a gas flow that removes the gaseous product. The reaction is furthermore facilitated by the strong decrease of the energy values with temperature. It is noted that commercially available chlorides, including LiCl, are known to contain trace amounts of oxide as one of their main impurities [25, 26].

Reactions 5 and 6 may help to elucidate why the final evaporation temperature of LiCl found in the experiments using small quantities is so far below the nominal boiling point of the material. As observed in Fig. 10, with increasing heating rate from  $10$  to  $50\text{ }^{\circ}\text{C min}^{-1}$ , the intensities of the peaks related to Reactions 5 and 6 decrease gradually, while the temperature for complete evaporation increases from  $1,027$  to  $1,167\text{ }^{\circ}\text{C}$  for 20 mg of LiCl. Conversely, according to Fig. 8, when increasing the mass from 9 to 42 mg, peak intensities for Reactions 3 and 4 decrease, while the temperature of final evaporation increases from  $1,072$  to  $1,218\text{ }^{\circ}\text{C}$  for the heating rate of  $40\text{ }^{\circ}\text{C min}^{-1}$ . Hur et al. found that LiCl containing  $0.11\text{ mol\%}$  of  $\text{Li}_2\text{O}$  evaporates completely at temperatures below  $1,150\text{ }^{\circ}\text{C}$ , and attributed this to a co-evaporation of LiCl and  $\text{Li}_2\text{O}$  in the form of an oxygen-bridged compound [27]. Based thereupon, the results of the present study can be explained. Increasing the heating rate causes Reactions 5 and 6 to occur to a lesser extent, thus yielding smaller concentrations of  $\text{Li}_2\text{O}$  in LiCl and smaller reductions of the final evaporation temperature. Increasing the mass of LiCl has an effect because Reactions 5 and 6 occur between a condensed phase and a gas phase, rendering their kinetics dependent on the surface-to-volume ratio of the condensed phase, so increasing the amount of LiCl leads to a relative decrease of surface area and reaction rate, and hence smaller concentrations of  $\text{Li}_2\text{O}$  in LiCl.

In the light of the above reasoning, the identical evaporation behaviour of LiCl when heated in argon and

ambient air, as shown in Fig. 6, may be attributed to the presence of water in both atmospheres, whilst the difference in oxygen content has no significant impact.

## Conclusions

Nominally anhydrous LiCl was found to absorb and retain approximately 2.55% of water after exposure to air at ambient conditions, forming a surface layer of mono-hydrate  $\text{LiCl}\cdot\text{H}_2\text{O}$ . Around 88% of the water content is removed by heating the material to 93–115 °C, depending on the heating rate applied. It was found that the de-hydration is governed by a two-stage mechanism at a heating rate of 10 °C min<sup>-1</sup> and by a one-stage mechanism at a heating rate of 20 °C min<sup>-1</sup> and above. Melting of the dehydrated LiCl occurred at temperatures very close to those quoted in the literature, indicating that the dehydration process leaves behind pure LiCl. Substantial evaporation of LiCl took place at temperatures far below its nominal boiling temperature, and it was found that the rate of evaporation increases gradually as the temperature approaches that required for complete evaporation. The present study for first time proposes the precise reactions that lead to oxide impurities in the molten LiCl, by linking the accelerated evaporation behaviour at temperatures in excess of 800 °C to the hydrolysis of LiCl and the subsequent decomposition of LiOH.

All transition temperatures of LiCl are affected to some extent by the heating rate, but only the evaporation process is affected critically by the quantity of the material employed and the flow rate of the gas passed over it. The transition temperatures do not depend on the type of gas atmosphere used, while the water content of the atmosphere has an effect on the evaporation behaviour of LiCl.

**Acknowledgements** The authors would like to thank R. Cornell and S.J. Griggs from the Department of Materials Science and Metallurgy, University of Cambridge, for their kind technical assistance.

## References

- Ebensperger A, Maxwell P, Moscoso C. The lithium industry: its recent evolution and future prospects. *Resour Policy*. 2005;30: 218–31.
- Karell EJ, Gourishankar KV, Smith JL, Chow LS, Redey L. Separation of actinides from LWR spent fuel using molten-salt-based electrochemical processes. *Nucl Technol*. 2001;136:342–53.
- Hur JM, Seo CS, Hong SS, Kang DS, Park SW. Metallization of  $\text{U}_3\text{O}_8$  via catalytic electrochemical reduction with  $\text{Li}_2\text{O}$  in LiCl molten salt. *React Kinet Catal Lett*. 2003;80:217–22.
- Iizuka M, Inoue T, Ougier M, Glatz JP. Electrochemical reduction of  $(\text{U}, \text{Pu})\text{O}_2$  in molten LiCl and  $\text{CaCl}_2$  electrolytes. *J Nucl Sci Technol*. 2007;44:801–13.
- Masset P, Guidotti RA. Thermally activated (“thermal”) battery technology. Part I: An overview. *J Power Sources*. 2006;161: 1443–9.
- Masset P, Guidotti RA. Thermal activated (thermal) battery technology. Part II. Molten salt electrolytes. *J Power Sources*. 2007;164:397–414.
- Winter M, Besenhard JO, Spahr ME, Novák P. Insertion electrode materials for rechargeable lithium batteries. *Adv Mater*. 1998;10:725–63.
- Sivakkumar SR, Nerkar JY, Pandolfo AG. Rate capability of graphite materials as negative electrodes in lithium-ion capacitors. *Electrochim Acta*. 2010;55:3330–5.
- Xu Q, Schwandt C, Chen GZ, Fray DJ. Electrochemical investigation of lithium intercalation into graphite from molten lithium chloride. *J Electroanal Chem*. 2002;530:16–22.
- Xu Q, Schwandt C, Fray DJ. Electrochemical investigation of lithium and tin reduction at a graphite cathode in molten chlorides. *J Electroanal Chem*. 2004;562:15–21.
- Sychev J, Borisenko NV, Kapitay G, Kushkhov KB. Intercalation of sodium and lithium into graphite as a first stage in an electrochemical method for producing carbon nanotubes. *Russ J Electrochim*. 2005;41:956–63.
- Sychev J, Kapitay G. Influence of current density on the erosion of a graphite cathode and electrolytic formation of carbon nanotubes in molten NaCl and LiCl. *Electrochim Acta*. 2009;54: 6725–31.
- Chen GZ, Fan XD, Luget A, Shaffer MSP, Fray DJ, Windle AH. Electrolytic conversion of graphite to carbon nanotubes in fused salts. *J Electroanal Chem*. 1998;446:1–6.
- Dimitrov AT, Chen GZ, Kinloch IA, Fray DJ. A feasibility study of scaling-up the electrolytic production of carbon nanotubes in molten salts. *Electrochim Acta*. 2002;48:91–102.
- Schwandt C, Dimitrov AT, Fray DJ. The preparation of nanostructured carbon materials by electrolysis of molten lithium chloride at graphite electrodes. *J Electroanal Chem*. 2010;647:150–8.
- Conde MR. Properties of aqueous solutions of lithium and calcium chlorides: formulations for use in air conditioning equipment design. *Int J Therm Sci*. 2004;43:367–82.
- Monnin C, Dubois M, Papaiconomou N, Simonin JP. Thermodynamics of the  $\text{LiCl} + \text{H}_2\text{O}$  system. *J Chem Eng Data*. 2002; 47:1331–6.
- Masset PJ. Thermogravimetric study of the dehydration reaction of  $\text{LiCl}\cdot\text{H}_2\text{O}$ . *J Therm Anal Calorim*. 2009;96:439–41.
- Kissinger HE. Variation of peak temperature with heating rate in differential thermal analysis. *J Res Nat Bur Stand*. 1956;57:217–21.
- Kissinger HE. Reaction kinetic in differential thermal analysis. *Anal Chem*. 1957;29:1702–6.
- Boonchom B, Danvirutai C. Rapid synthesis, kinetics and thermodynamics of binary  $\text{Mn}_{0.5}\text{Ca}_{0.5}(\text{H}_2\text{PO}_4)_2\cdot\text{H}_2\text{O}$ . *J Therm Anal Calorim*. 2009;98:717–23.
- Danvirutai C, Noisong P, Youngme S. Some thermodynamic functions and kinetics of thermal decomposition of  $\text{NH}_4\text{MnPO}_4\cdot\text{H}_2\text{O}$  in nitrogen atmosphere. *J Therm Anal Calorim*. 2010;100:117–24.
- Roine A. Outokumpu HSC chemistry for windows-chemical reaction and equilibrium software with extensive thermochemical database: Version 5.0. Outokumpu Research Oy Information Service, Finland; 2002.
- Kubaschewski O, Alcock CB, Spencer PJ. Materials thermochemistry. 6th ed. Oxford: Pergamon Press; 1993.
- Nitsch K, Dušek M, Nikl M, Polák K, Rodová M. Ternary alkali lead chlorides: crystal growth, crystal structure, absorption and emission properties. *Prog Cryst Growth Charact*. 1995;30:1–22.
- Smirnov MV, Korzun IV, Oleynikova VA. Hydrolysis of molten alkali chlorides, bromides and iodides. *Electrochim Acta*. 1988;33:781–8.
- Hur JM, Park SB, Seo CS, Jung KJ, Park SW. Melting and vaporization of salts in a U-LiCl-Li<sub>2</sub>O system. *J Radioanal Nucl Chem*. 2006;270:489–93.